Reduction of Main Beam-Blockage in an Integrated 5G Array with a Metal-Frame Antenna

Rodriguez Cano, Rocio; Zhang, Shuai; Zhao, Kun; Pedersen, Gert F.

Published in:
I E E E Transactions on Antennas and Propagation

DOI (link to publication from Publisher):
10.1109/TAP.2019.2900407

Publication date:
2019

Document Version
Accepted author manuscript, peer reviewed version

This article has been accepted for publication in a future issue of this journal, but has not been fully edited. Content may change prior to final publication. Citation information: DOI 10.1109/TAP.2019.2900407, IEEE Transactions on Antennas and Propagation

Reduction of Main Beam-Blockage in an Integrated 5G Array with a Metal-Frame Antenna

Rocio Rodriguez-Cano, *Student Member, IEEE*, Shuai Zhang, *Senior Member, IEEE*, Kun Zhao and Gert Frølund Pedersen, *Senior Member, IEEE*

***Abstract*—In this paper, a novel technique is introduced to reduce the handset metal-frame blockage to the main beam of a millimeter-wave (mm-wave) end-fire antenna array. The metal-frame blockage to mm-wave antennas with different polarizations is investigated first. It is found that the blockage is more severe for horizontal polarization than for vertical polarization. The effect of the metal bezel on a mm-wave array with horizontal polarization can significantly be decreased if two tilted layers of coupled metal strips are placed at the borders of the frame. Furthermore, these metal strips are shown not to disturb mm-wave antennas with vertical polarization. Different detailed design considerations are studied. To further demonstrate the idea, a 5G Vivaldi array (with horizontal polarization) is designed and integrated with a metal frame. The frame functions as a low-frequency antenna, operating in two frequency bands of 865-990 MHz and 1358-2786 MHz. The millimeter-wave array with four elements operates at the frequency band 24.25-27.5 GHz and can scan $\pm$60 degrees in end-fire direction, with a realized gain higher than 7 dBi in most of the frequency range.**

***Index Terms*—5G mobile communication, antenna array, millimeter wave integrated circuit, Vivaldi antennas.**

I. Introduction

THE upcoming fifth generation of mobile communications (5G) proposes more frequency bands to cope with the exponential demand of capacity and data traffic [1]–[4]. The millimeter-wave (mm-wave) band presents several challenges in terms of propagation. Since the propagation losses increase with frequency, higher gain antenna systems are required in mm-wave bands. As a result of the increased gain, the beamwidth becomes narrower and consequently, arrays are needed to steer the beam throughout the sphere. Electronic beam-steering is the most compact approach for mobile devices. There are two methods to steer the beam electronically; the first consists of switching the antennas [5], [6] and the other involves changing the relative phases of the signals which drive each antenna element (phased arrays) [7]–[13]. It is also possible to combine both methods by having several sub-arrays [8]–[11].

5G-enabled handsets need to include antennas operating at these new frequency ranges. The current tendency in mobile terminals is to include an increasing amount of components in small spaces. Because of the decreasing volume left in the phone, a good approach is to integrate the new mm-wave antennas with the existing ones. Many antenna designs for mobile terminals at mm-wave frequencies present end-fire radiation since they have higher spherical coverage [14] and are less sensitive to user effects in mm-wave bands [12], [15]. Conventional handsets with metal-frame designs have become a dominant trend nowadays. However, none of the previous designs in [5], [8], [9], [12]–[16] takes the handset metal frame into account. When a metal frame is placed in front of mm-wave end-fire antennas, severe distortion of the radiation pattern may occur due to the main beam blockage. This degradation can be translated into a shrinkage of the end-fire radiation bandwidth or a full deterioration of the pattern to broadside or other directions.

In [16], a layer of grating strips is added to obtain end-fire radiation, when a planar inverted-F antenna (PIFA) is placed in front of the high-frequency antenna. In this case, the operating mechanism is similar to the optical interferometers [17]. The distance between the grating strips and the PIFA is designed to be a quarter wavelength at a certain frequency and the end-fire radiation can be achieved within a band around that frequency. However, the bandwidth in which the antenna can remain with a stable end-fire radiation pattern would become very narrow when applying this technique for a metal-frame handset. In [7], [18], [19], mm-wave slot arrays have been etched on a metal frame, and the end-fire beams are not blocked by the bezel anymore. Nevertheless, in order to excite these slots, the feeding cable (or other transmission lines) has to connect the PCB ground to the metal bezel. This would change the low-frequency antenna performance if a metal bezel antenna at sub 3 GHz is applied. Moreover, introducing additional feeding structures to the metal bezel would also complicate the practical implementations. Therefore, it is necessary to propose a technique which is able to reduce the main beam blockage in an integrated end-fire 5G array with a metal-frame antenna operating at low frequencies.

In this paper, a mm-wave Vivaldi antenna array (with end-fire radiation pattern) is integrated together with a metal-frame antenna at sub 3 GHz. Two layers of coupled metal strips are introduced to overcome the directional obstruction of the metal frame to the main beam of the Vivaldi array. These metal strips do not alter the performance of the metal-frame antenna. The mm-wave antenna array is designed to operate at the 5G pioneer band in Europe, from 24.25-27.5 GHz [20]. Simulations are carried out by CST Microwave Studio 2018 and a prototype is manufactured and measured.

This work was supported by the InnovationsFonden project of Reconfigurable Arrays for Next Generation Efficiency (RANGE).

Rocio Rodriguez-Cano, Shuai Zhang, Kun Zhao and Gert F. Pedersen are with the Antenna, Propagation and Millimeter-Wave Section (APMS) at the Department of Electronic Systems, Aalborg University, 9220 Aalborg, Denmark. Corresponding author Shuai Zhang (e-mail: sz@es.aau.dk).

Kun Zhao is also with Research and Standardization, Sony Mobile Communications, Lund, Sweden.

This article has been accepted for publication in a future issue of this journal, but has not been fully edited. Content may change prior to final publication. Citation information: DOI 10.1109/TAP.2019.2900407, IEEE Transactions on Antennas and Propagation

The manuscript is organized as follows; Section II introduces the degradation produced by the mobile phone frame in the radiation pattern of horizontally polarized antennas and the effect of the frame width. Section III describes the operating mechanism and the proposed structure to overcome this problem. Design considerations are also explained. In Section IV, the final parameters of the antenna design are listed and the performance is assessed, with measurements and simulations.

II. Effect of the Metal Frame on mm-Wave Antennas

As mentioned in the introduction, the metal frame of mobile devices may block the radiation from the end-fire antennas in the mm-wave frequency range. In order to provide a clear picture of this point, the impact of the metal frame on the radiation pattern of mm-wave antennas is analyzed. First, according to the polarization and then, with a parametric study of the frame width.

A. Polarization dependence of the metal-frame blockage to the radiation pattern

In 5G mobile handsets, mm-wave antenna arrays with dual polarization are preferred. In this section, the metal-frame blockage to different polarizations is investigated. To carry out this study, two patches, one with vertical polarization (Fig. 1 (a)) and the other with horizontal (Fig. 1 (b)), are placed 7 mm away from a 5 mm-wide frame, which is the typical clearance in handsets. Please note that the frame width referred throughout this paper is the dimension in the z axis.

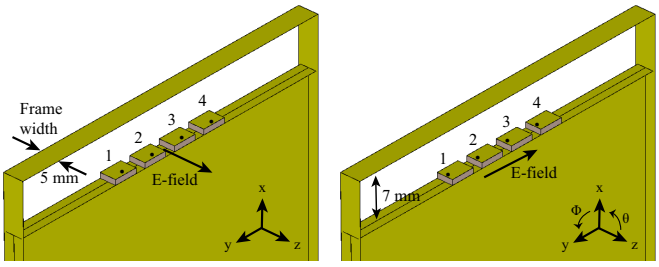

(a) (b)

Fig. 1. Simulated patch antennas with frame and ground plane. (a) Vertical polarization. (b) Horizontal polarization.

The effect of the frame on the radiation patterns of vertical and horizontal polarizations are shown in Fig. 2 and Fig. 3, respectively. The radiation patterns are obtained by exciting the third element of the array with the others terminated with 50 Ω loads. The realized gain of two perpendicular cuts is plotted in the figures. In Fig. 2, when a metal frame is included, the vertically-polarized patch has some energy reflected back, but the main beam still points to the end-fire direction and the radiation patterns do not vary significantly. However, as plotted in Fig. 3, the main direction of radiation in horizontal polarization is much more sensitive to the frame than the vertical polarization. There is also a loss of more than 6 dB in the $+x$ axis ($\phi = 0°$ and $\theta = 90°$). The reason for the severe blockage to the horizontal polarization may be explained as follows: the wavelength at the center frequency of the band, 26 GHz, is over one time longer than the frame width (5 mm). For the horizontal polarization, the amplitude of the electric field varies in the y axis, which is totally blocked by the metal frame (see Fig. 1). In the case of vertical polarization, the amplitude of electric field varies in the z axis, not in the y axis, and thus the wavefront is only partially obstructed.

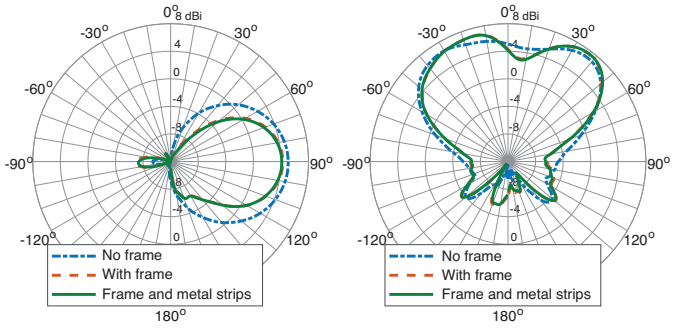

(a) (b)

Fig. 2. Effect of the parasitic metal strips on the realized gain radiation patterns of vertical polarization at 26 GHz. (a) $\phi = 0°$ cut. (b) $\theta = 90°$ cut.

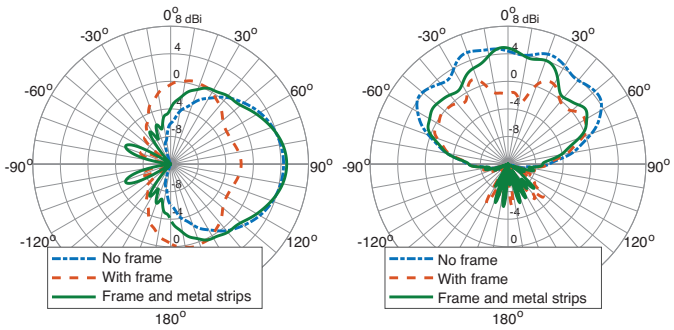

(a) (b)

Fig. 3. Effect of the parasitic metal strips on the realized gain radiation patterns of horizontal polarization at 26 GHz. (a) $\phi = 0°$ cut. (b) $\theta = 90°$ cut.

Since the degradation of the radiation pattern when the frame is added is not significant for vertical polarization, from now on, only the case of horizontal polarization is assessed.

B. Effect of the frame width

The contribution of the frame width to the degradation of the radiation pattern is plotted in Fig. 4. Only the gain (IEEE) radiation patterns of the central element are shown. The IEEE definition of gain equals the antenna directivity plus the antenna radiation efficiency in logarithmic scale, and thus the mismatching loss is not included. As the width increases, the energy in the end-fire direction decreases and more energy reflects in other directions. This effect is even more noticeable when the width is larger than 2 mm.

Therefore, it can be concluded that the blockage effect of the metal frame is more critical for the radiation pattern in the case of the horizontal polarization than the vertical. In the

This article has been accepted for publication in a future issue of this journal, but has not been fully edited. Content may change prior to final publication. Citation information: DOI 10.1109/TAP.2019.2900407, IEEE Transactions on Antennas and Propagation

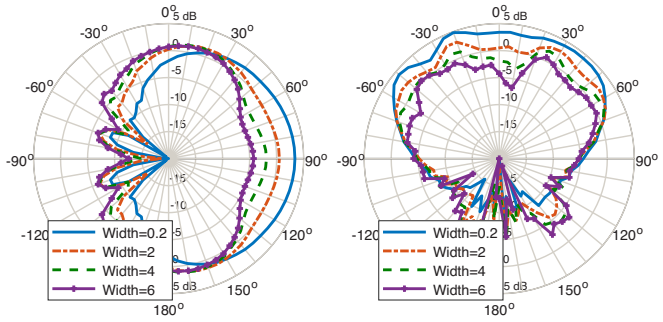

(a) (b)

Fig. 4. Effect of the frame width in the gain (IEEE) radiation pattern at 26 GHz. (a) $\phi = 0°$ cut. (b) $\theta = 90°$ cut. See coordinates in Fig. 1.

next section, a novel technique is introduced to overcome this blockage.

III. Metal Strip Layers Coupled to the Frame

As stated in the previous section, mm-wave end-fire arrays with horizontal polarization face a degradation of the radiation pattern when the metal frame is added in a handset. To overcome this problem, coupled strip layers are introduced in this section.

To illustrate the polarization impact, a patch antenna was chosen. Nevertheless, one of the main drawbacks of patch antennas is their narrowband impedance matching. In order to cover the band n258 of the mm-wave spectrum, a wideband, high-gain antenna with robust radiation pattern is needed. The Vivaldi element is a good reference antenna to study in the presence of the frame, due to its high gain and stable radiation pattern in a wide band. For that reason, in the rest of the paper, the Vivaldi antenna is analyzed.

A. Fundamental mechanism

The concept of the coupled strip layers consists of two tilted strips placed at both sides of the frame, as shown in Fig. 5 (a). The mm-wave antenna radiates towards the frame. A portion of the energy is reflected back, but the larger part is coupled to the metal strip layers. The two metal strip layers work as parasitic radiators, which re-radiate the electromagnetic waves coupled from the two edges of the metal frame towards the original direction. Since the distance from the mm-wave antenna to each metal strip layer is the same, the electromagnetic waves re-radiated are added in phase, which combines into end-fire radiation pattern again in the far-field. In other words, the strips can be regarded as two radiating sources fed by the coupling of the energy from the frame. The electric field propagation is represented in Fig. 5 (b) at a time instant for a frequency of 26 GHz. The first wavefront can be seen at the left side of the picture, originated by the sum of the coherent radiation from the parasitic strips. The strip layers are required to be close to the frame to acquire enough coupled energy. This is one of the differences with the optical interferometer, in which the distance is required to be around a quarter wavelength [17].

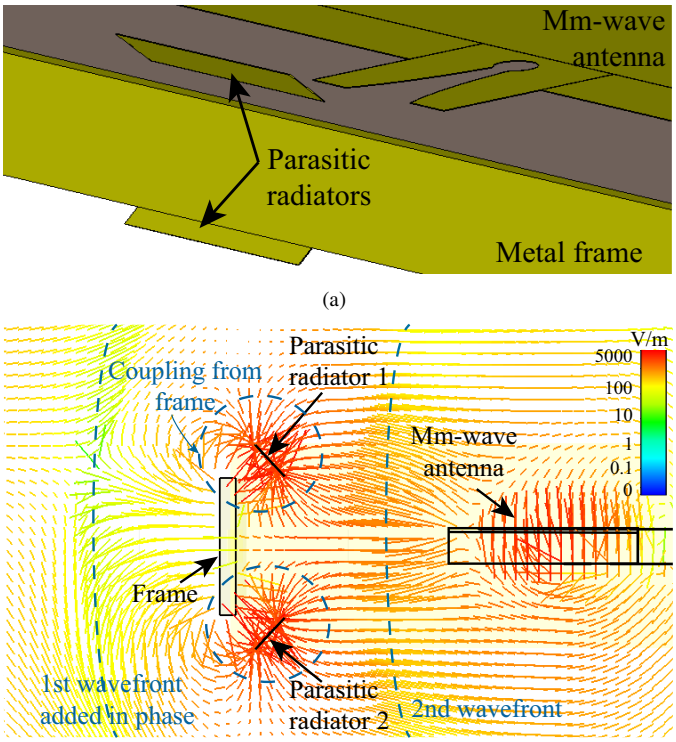

Fig. 5. (a) Mm-wave antenna with frame and metal strips. (b) E-field of the mm-wave antenna with frame and metal strip layers (side view).

B. Impact of the coupled strip layers in the radiation of an antenna array

To compensate the high path losses in the mm-wave band, antenna arrays are proposed to be embedded in mobile terminals. The principle of adding strips at both sides of the frame can be extended for the array case. The purpose of the mm-wave array is steering the beam to provide a good coverage of the upper hemisphere. For that reason, each layer is composed of many strips. Fig. 6 shows the two layers at both sides of the frame with several metal strips.

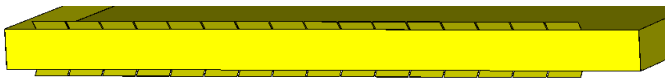

Fig. 6. Front view of the metal strip layers for the mm-wave array.

To further demonstrate this concept, the surface current of the Vivaldi array has been plotted along the frame with and without metal strips layers in Fig. 7. It can be seen in Fig. 7 (a) that the currents flow as standing waves, while in Fig. 7 (b) the currents are coupled along the edges to the metal strip layers and become weak close to the center of the frame.

The previous subsection introduced the operating principle of the strip layers. For a better comprehension of the mechanism, the effect of the number of strip layers is assessed below. Fig. 8 (a) represents the radiation patterns of the Vivaldi array with no frame (in free-space) with all the elements excited in phase. Fig. 8 (b) shows the effect of the frame on the radiation pattern of the array. The width of the metal frame in front of

This article has been accepted for publication in a future issue of this journal, but has not been fully edited. Content may change prior to final publication. Citation information: DOI 10.1109/TAP.2019.2900407, IEEE Transactions on Antennas and Propagation

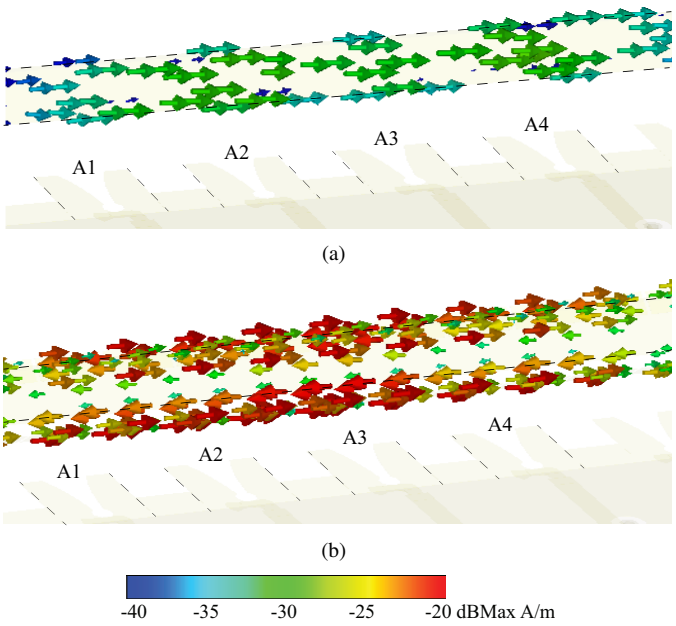

Fig. 7. Surface current comparison in dBA/m with respect to the maximum value at 26 GHz. (a) Without metal strip layers. (b) With metal strips.

the array (top part) is set to be 3 mm in this study. The frame decreases the gain of the array by at least 3 dBi at the two higher frequencies, and by more than 4 dBi at 24.25 GHz. If only one layer of metal strips is added close to the edge of the frame (Fig 8 (c)), the IEEE gain in the end-fire direction ($+x$ axis) is improved at 24.25 GHz, but the sidelobes decrease the gain at the higher frequencies. Nonetheless, placing two layers of strips redirects the radiation to the $+x$ axis direction across the target bandwidth, as shown in Fig. 8 (d). This happens due to the coupling of the electromagnetic wave from the frame to the metal strips. The metal layers radiate the coupled energy to the desired end-fire direction. Fig. 9 shows the IEEE gain of the array at the $+x$ axis for the different number of metal strip layers placed at the edges of the frame. The IEEE gain when one layer of metal strips is added is higher than the one with only frame at the lower frequencies of the band, but when the frequency increases, the side lobes have higher value. The improvement in the gain is more significant when the two layers are placed since the two metal layers act as two elements of an array.

In order to show that the strip layers do not affect the vertical polarization, the plots of the patch antenna with strip layers have also been included in Fig. 2 and 3 for both polarizations. Simulations show that the realized gain, for the vertical polarization, does not vary when the two coupled metal strips layers have been placed next to the borders of the frame (Fig. 2). This means that the parasitic strips do not degrade the vertical polarization. The improvement of the gain is about 7 dBi in the case of horizontal polarization (Fig. 3) compared to the structure with only the frame. The main beam points again to the original direction ($+x$ axis).

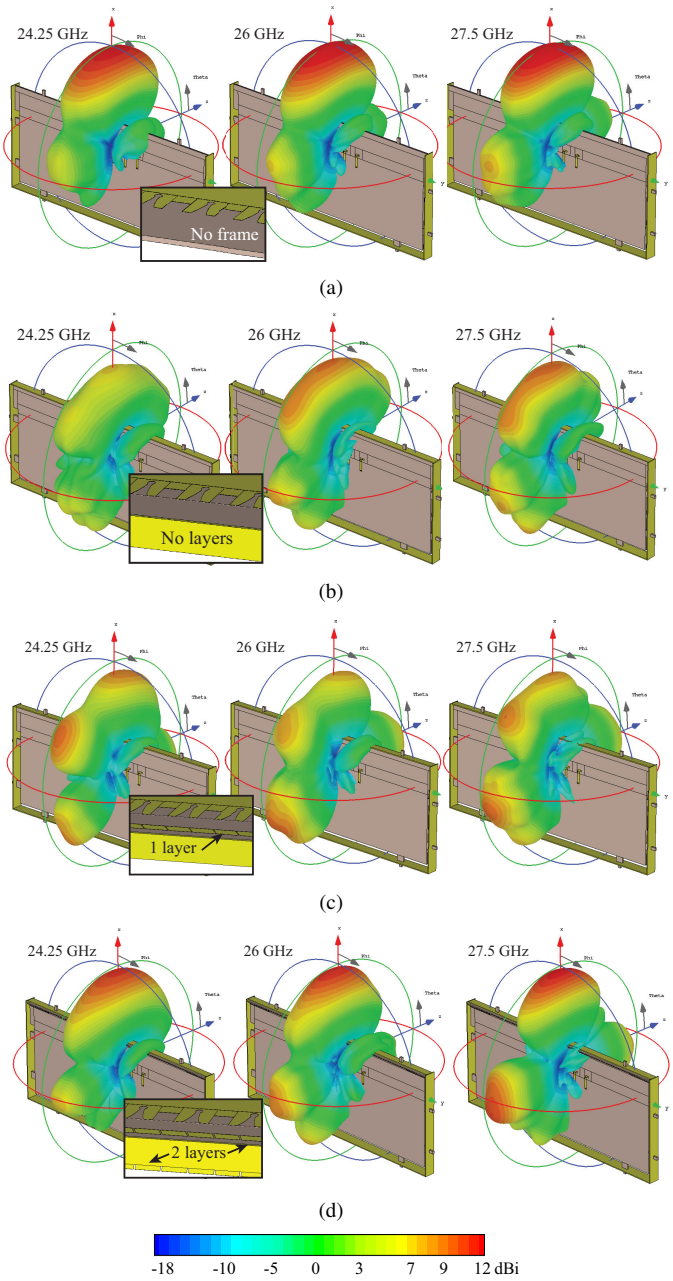

Fig. 8. IEEE gain comparison of the in-phase Vivaldi array according to the number of layers of metal strips at different frequencies. (a) No frame. (b) No layers. (c) 1 layer. (d) 2 layers.

C. Design considerations for the integration of a mm-wave array and a metal frame-antenna

The principle and effectiveness of the coupled metal strip layers have been demonstrated in previous section. In this section, several considerations for the design of the integrated mm-wave array with the frame antenna are investigated, such as angle of the strip layers, gap between the strips, strip length and antenna-frame distance. The optimal configuration for the integration of a mm-wave array and a metal frame antenna can be revealed through the parametric studies. In addition, it should be noticed that, in all the sweeps, IEEE gain is used instead of realized gain. The IEEE gain is adopted to

This article has been accepted for publication in a future issue of this journal, but has not been fully edited. Content may change prior to final publication. Citation information: DOI 10.1109/TAP.2019.2900407, IEEE Transactions on Antennas and Propagation

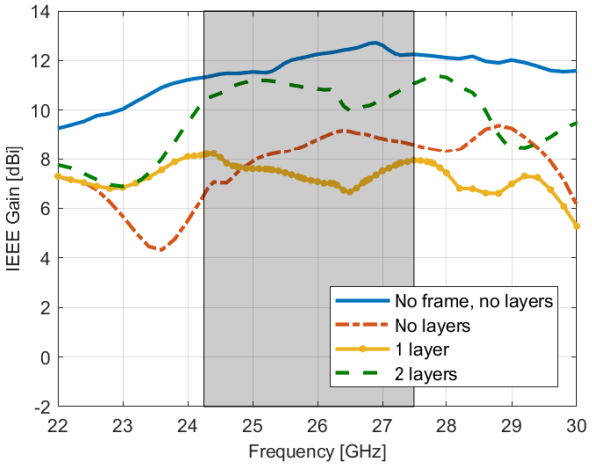

Fig. 9. End-fire IEEE gain (in the $+x$ axis) of the array according to the number of metal strip layers as a function of the frequency.

exclude the changes in the antenna impedance matching for some configurations, which provides a fair comparison. The matching is, however, better than -6 dB in the worst case.

1) Effect of the angle of the strip layers: The IEEE gain of the array in the $+x$ axis has been represented in Fig. 10 for different angles of the strip layers. The rotation is made by fixing the edge of the layer that is further away from the frame (see Fig. 10). The gain variation is not significant in all the cases but when the layers are parallel to the frame. This means that even if the layers are not perfectly aligned forming an angle of $45°$, the gain would not vary significantly. This result shows that the angle is not a critical parameter for the design. Similarly, from our studies, the strip-frame distance is not a critical parameter either. In practice, if the phone is dropped, in the worst case, the strip layers angle or the strip-frame distance would be slightly changed or shifted. This would have a very limited impact on the antenna performance.

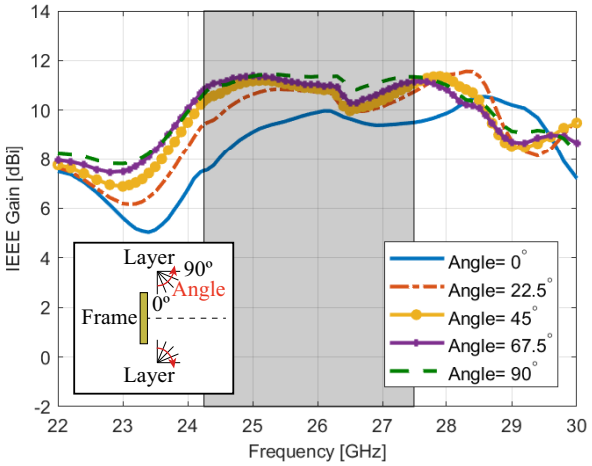

Fig. 10. End-fire IEEE gain (in the $+x$ axis) of the array depending on the angle of inclination of the strip layers.

2) Effect of the gap between the strips: The spacing between the different metal strips is one of the most sensitive parameters. The inter-strip gap mainly affects the mutual coupling between strip elements, which contributes to providing a wider bandwidth with end-fire radiation pattern. It can be observed from Fig. 11 that a stable high gain in the end-fire direction is obtained over a wide band by properly adjusting the inter-strip gap or coupling. Decreasing the gap shifts the resonant peaks down in frequency. Therefore, the width of the gap needs to achieve the maximum gain in the frequency band (shadowed area). Moreover, the gap needs to be wide enough to ensure the fabrication viability. Fig. 11 shows that a gap of 0.15 mm provides the highest gain in all the frequency range. This gap width can be precisely obtained with the milling tools available.

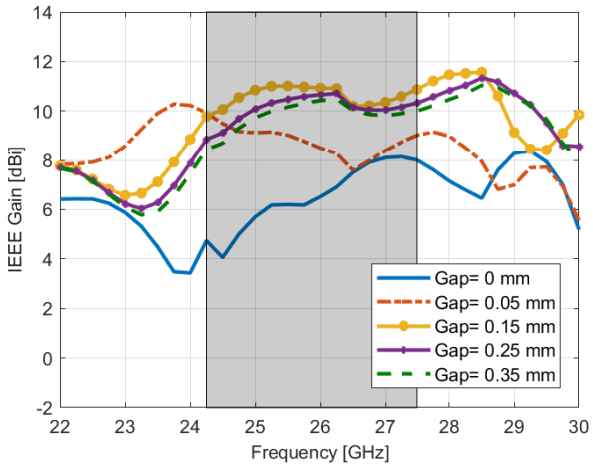

Fig. 11. End-fire IEEE gain (in the $+x$ axis) of the array depending on the gap between the strips.

3) Effect of the strip length: A sweep in the metal strips length is presented in Fig. 12 and it is also a critical design parameter. The gap width is kept constant in the simulations, with a value of 0.15 mm. The tendency of the gain with the length is the opposite than with the gap. If the strip length is decreased, the gain curve in the $+x$ axis shifts to higher frequencies. The reason for this behaviour is because the strips act as parasitic radiating elements. Thus, a higher gain in the operating band can be obtained with a shorter strip length. The length which provides the best gain in the end-fire direction ($+x$ axis), corresponds to 2.55 mm.

4) Effect of the frame-antenna distance: The mm-wave-antenna distance to the frame is another parameter that needs consideration. The clearance is a limitation in the design of mm-wave antennas. However, as Fig. 13 shows, when the frame is too close to the antenna more energy is reflected and therefore, the gain is lower. If the top part of the antenna is located at 7 mm from the frame, the gain exhibits better performance in almost all the bandwidth. The metal strip layers are included in this study and all the elements are excited in phase. The proposed mechanism is valid for any clearance since the gain is higher with the strip layers than with just the frame (both at 2 and 7 mm away). Moreover, the gain enhancement increases even more with a smaller clearance (e.g. there is a 5 dB increase in a wide band with $d = 2$ mm

This article has been accepted for publication in a future issue of this journal, but has not been fully edited. Content may change prior to final publication. Citation information: DOI 10.1109/TAP.2019.2900407, IEEE Transactions on Antennas and Propagation

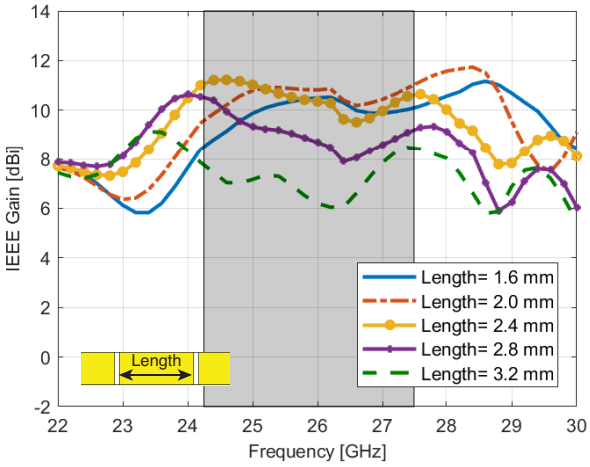

Fig. 12. End-fire IEEE gain (in the $+x$ axis) of the array with two metal strip layers for different lengths as a function of the frequency.

compared with the solution without metal strips).

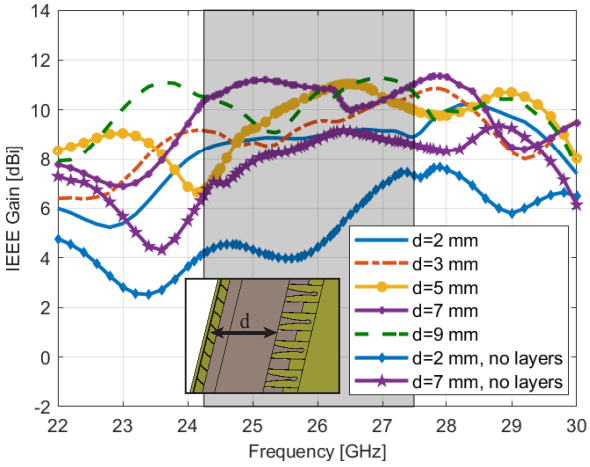

Fig. 13. IEEE gain comparison for different distances from the mm-wave array to the frame.

To sum up, the gap width and strip length have been shown to be the most critical parameters in the design of the strip layers. The angle of the strip layers does not significantly modify the gain in the $+x$ axis. Finally, the strip layers improve the gain of the structure with respect of no layers at all, especially for smaller clearances.

IV. Final Design and Performance

Through the parameter studies in the previous section, an optimized Vivaldi array with coupled metal strip layers is obtained. A complete design together with a low-frequency metal-frame antenna at sub-6 GHz is presented in this section. The authors would like to emphasize that the antenna-frame distance has been set to 7 mm because of design constraints of the low-frequency antenna. The proposed antenna and its prototype are shown in Fig. 14 and Fig. 15, respectively. The proposed antenna is composed by a low-frequency metal-frame antenna and a mm-wave Vivaldi array with coupled metal strips. In order to attach the frame to the PCB in the precise location, protrusions etched in the PCB need to be inserted in the holes along the perimeter of the bezel as support spacer (see Fig. 14 (a)). The supports are only made to facilitate the manufacturing of the prototype and it is not required in practical applications. Fig. 15 (a) corresponds to the prototype without the coupled metal strip layers. Due to the tilted nature of the metal strips, a supporting foam is added to ensure the right inclination (Fig. 15 (b)) in the manual fabrication. The metal strip layers are pasted on the inner face of the foam support, as illustrated in Fig. 15 (c), and then placed on both sides of the substrate, as Fig. 15 (d) shows. The top part of the handset frame is slightly narrower than the rest, so the black sections at both sides of the top frame correspond to the strip layers (the strips are facing the foam). The pliability of the foam used to verify the proposed idea can be avoided in practical massive production, where the metal strips, mm-wave antennas, and low-frequency antenna would be integrated together with precision.

A. Dual-loop metal-framed antenna

As shown in Fig. 14 and Fig. 15, the geometry of the low-frequency antenna is an unbroken metallic frame that covers the edges of the handset. The dual-loop antenna is formed when the ground plane of the PCB is combined with the rimmed-strip. The PCB is grounded on one of the protrusions on the right side, to form two loops. A 0.5λ mode is generated at 518 MHz and 985 MHz for the first and second loop, respectively. High-order resonant modes of both loops are also excited, and their combination provides a wide impedance bandwidth. The design of the bezel antenna is based on the configuration in [21], but any other wideband metal-frame antennas can be employed. The width of the frame is 5 mm on the left, right and bottom sides, and 3 mm on the top side. The reason for making the top part narrower is to make sure that the highest point in the metal layers does not stand out from the 5 mm-wide frame. The thickness of the bezel is 0.3 mm. The total dimensions of the phone are 155.7 mm $\times$ 88.6 mm. The feeding (port 5) is a coaxial cable that connects the PCB with the frame (see Fig. 15 (a)) and is located at 29 mm from the top part of the substrate.

The low-frequency antenna has been measured and the reflection coefficient is represented in Fig. 16. The matching criterion for the low-frequency antenna is -6 dB. The measured impedance bandwidth covers the bands of 822-995 MHz, 1338-2321 MHz and 2429-2780 MHz. The bandwidth and radiation pattern of the metal frame antenna do not change when the metal strip layers are added. The simulated mutual coupling between the low-frequency antenna and the mm-wave array is below -40 dB in the low band and -32 dB in the operating mm-wave band. The total efficiency does not vary either with the coupled metal layers, and its value is 75 %, 85 % and 80 % for the respective bands. Therefore, the coupled metal strip layers do not change the performance of the low-frequency antenna.

This article has been accepted for publication in a future issue of this journal, but has not been fully edited. Content may change prior to final publication. Citation information: DOI 10.1109/TAP.2019.2900407, IEEE Transactions on Antennas and Propagation

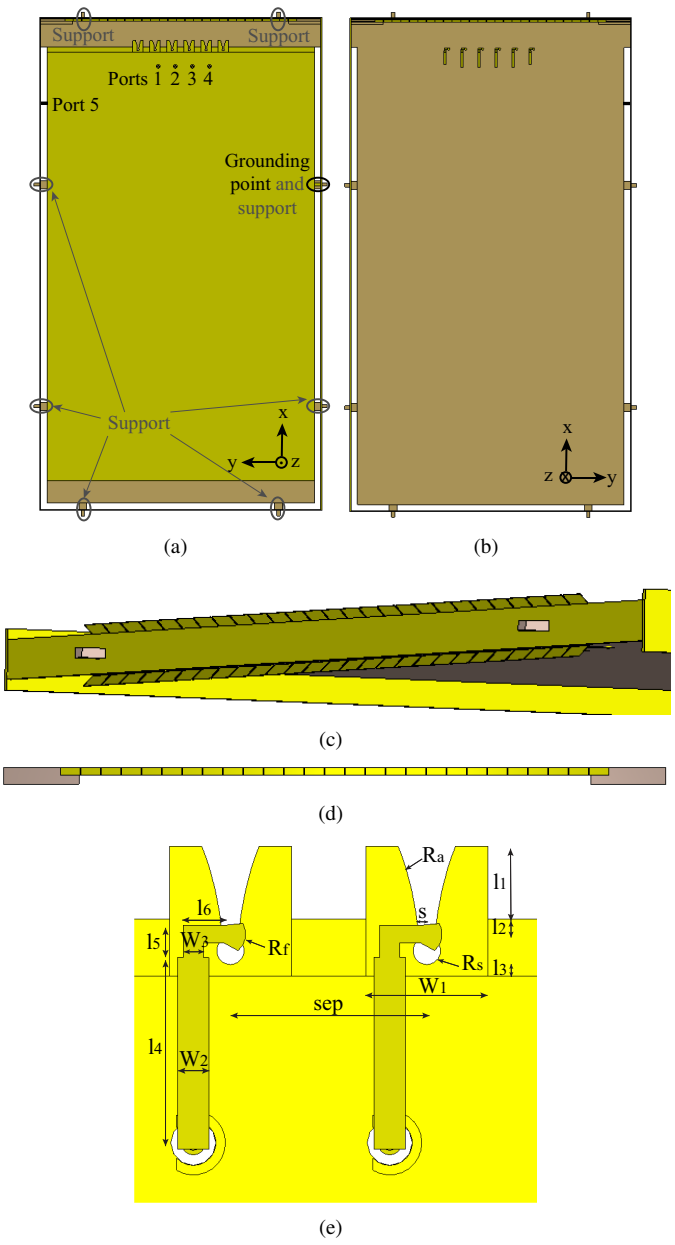

Fig. 14. Proposed handset antenna. (a) Top view. (b) Bottom view. (c) Zoomed view of the metal strip layers with their substrate hidden. (d) Coupled metal strip layer. (e) Geometry of the Vivaldi antenna.

B. Mm-wave Vivaldi array with coupled metal layers

The geometry of the mm-wave array is shown in Fig. 14. The array is composed of 4 active Vivaldi elements and two dummy grounded elements to ensure the similar boundary conditions for all the driven elements, and therefore match the edge elements in the array [22]. The Vivaldi element has overall dimensions of 3.31 mm $\times$ 3.61 mm, and it is implemented on Rogers RO3006 substrate with a dielectric permittivity of 6.15 and thickness of 0.64 mm. The Vivaldi antenna is fed by a microstrip line ended with a radial stub [23], but other feeding methods like SIW [24] can be employed. The coupled metal strip layers are etched on CuClad 217 substrate of $\epsilon_r = 2.17$ and thickness of 0.254 mm to facilitate the fabrication. As discussed in the previous section,

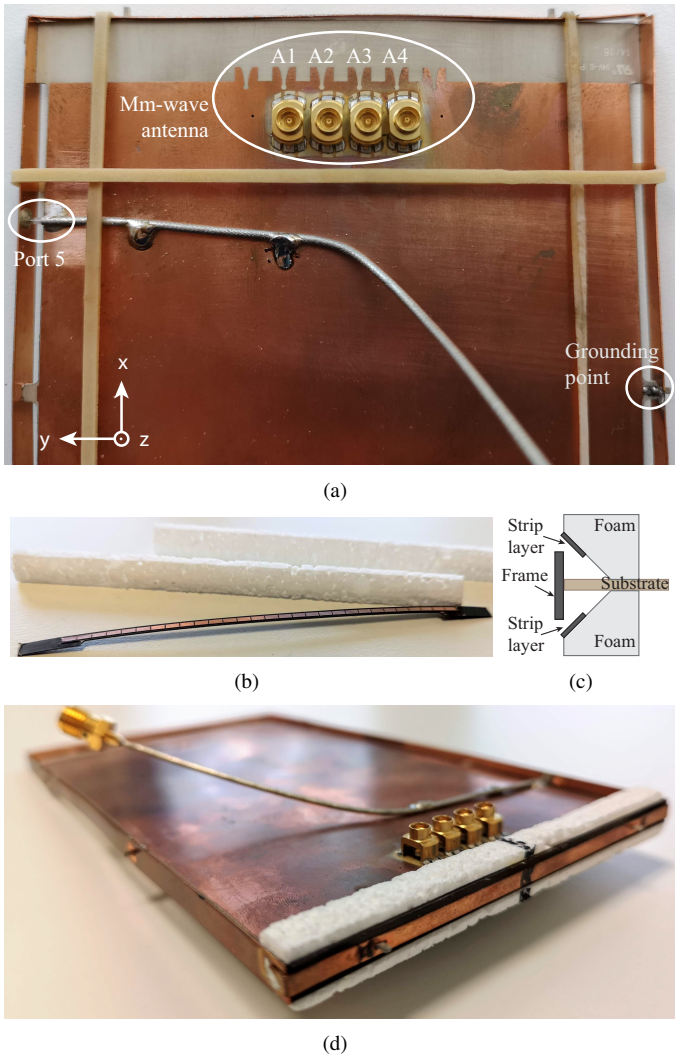

Fig. 15. Antenna prototype. (a) Antenna without metal strip layers. (b) One of the metal strip layers and foam support structures. (c) Detailed scheme of the *xz* plane with the strip layers placement. (d) Final mounted structure.

the important design parameters are the gap of the metal strips (s_g) and the length (l_g). The tilting angle is fixed to ($45°$). The final dimensions of the antenna are listed in Table I. The measurements and simulated results of the integrated high-frequency array are discussed in the next paragraphs.

TABLE I
DIMENSIONS OF THE VIVALDI ANTENNA ARRAY AND THE COUPLED METAL STRIP LAYERS (UNIT: MM)

Parameter	Value	Parameter	Value
R_a	0.53	l_5	0.38
s	0.21	l_6	1.11
l_1	2.48	w_2	0.84
l_2	0.05	w_3	0.53
l_3	1.07	R_f	0.58
R_s	0.37	α_f	80°
sep	5.35	l_g	2.4
w_1	3.31	w_g	1
l_4	5.21	s_g	0.15

A comparison between simulated and measured S_{11} of the antenna without frame and metal strip layers and the complete

This article has been accepted for publication in a future issue of this journal, but has not been fully edited. Content may change prior to final publication. Citation information: DOI 10.1109/TAP.2019.2900407, IEEE Transactions on Antennas and Propagation

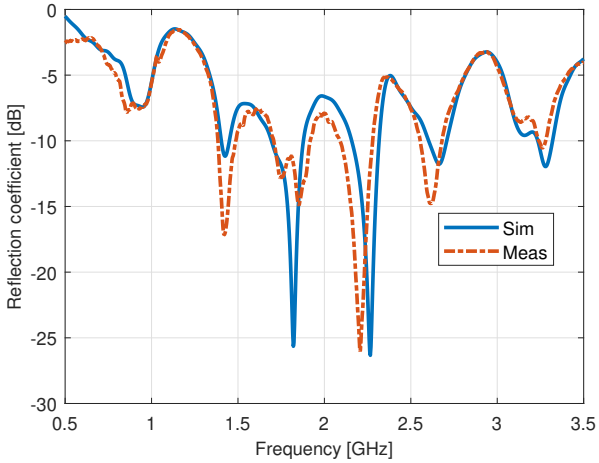

Fig. 16. Comparison of the reflection coefficient of the low-frequency antenna.

designed structure is plotted in Fig. 17 (a). The criterion considered for impedance matching at high frequencies is a reflection coefficient of -10 dB. Good agreement can be observed between simulations and measurements, where the measured bandwidth is only shifted 1.92 % to lower frequencies. The presence of the frame and metal strips layers reduces the impedance bandwidth around 2.69 %, but it is still wide enough to cover the 5G band n258 specified in 3GPP, as well as the n261 band [20]. Fig. 17 (b) shows a comparison of the S-parameters of the antenna elements A1 and A2 (see Fig. 15 (a)). The reflection coefficient of the antenna elements A3 and A4 is similar. The mutual coupling in the worst case (A2 with A3) is lower than -11 dB through the whole bandwidth.

The set-up for the radiation pattern measurement is shown in Fig. 18. A horn is used as a probe in the measurement system. Each antenna element is measured at a time, with the rest of the elements loaded with 50 Ω. The measured antenna is located in a platform that can rotate 360°, and the mechanical arm, where the horn is fixed, can move from $\theta = 0°$ to 135°. The radiation pattern in the H-plane has been plotted in Fig. 19 for the elements A1 and A2 (antenna numbering is specified in Fig. 15 (a)). The radiation patterns point to the $+x$ axis, which means that the antenna has end-fire radiation. The shape of the measured radiation patterns is similar to the simulations. The side lobe on the non-metal side ($\theta = -180°$) is a bit high, but it is due to the shape of the radiation pattern of the Vivaldi element, instead of the metal strip layers. The representation in the E-plane is shown in Fig. 20. A good agreement is found between measurements and simulations. However, the main lobe direction has been slightly shifted from the $+x$ axis. Therefore, the cuts represented do not include the maximum gain value. For that reason, in the measurements, the realized gain is slightly lower than the simulated at 26 GHz.

Fig. 21 represents the realized gain in the end-fire direction ($+x$ axis) as a function of the frequency. All the elements have been plotted individually and also the array is excited in phase. The realized gain is higher than 8 dBi in the whole the frequency range.

The resulting simulated beam-steering envelope is shown in Fig. 22. In order to obtain the envelope, the maximum realized gain of 13 beams is plotted at each angle of ϕ. The progressive phase shifts generated to obtain those beams are ±45°, ±60°, ±90°, ±105°, ±120° and ±135°. The array can scan ±60° with an average gain higher than 7 dBi for the entire frequency range.

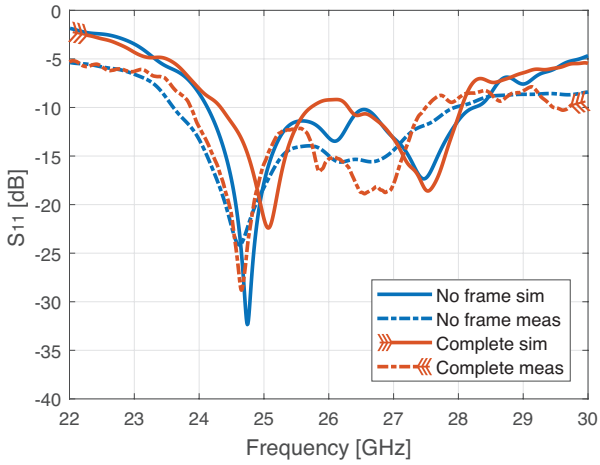

(a)

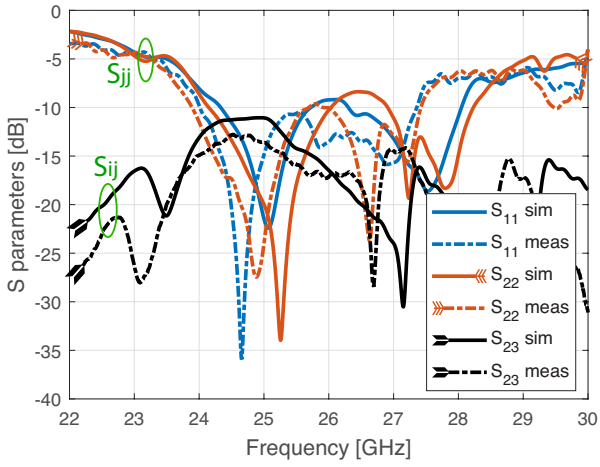

(b)

Fig. 17. S parameter comparison. (a) Reflection coefficient comparison between measurements and simulations of port 1. (b) Comparison between the S-parameters of measurements and simulations of the final design.

V. Conclusion

Mm-wave horizontally-polarized end-fire antenna arrays face a degradation of the main beam when the metal frame of a phone is placed. In order to overcome this obstruction, coupled metal strip layers have been proposed to be located at both sides of the frame edge. The coupling between the frame and the tilted layers allows them to act as a relay, re-radiating the energy to the desired direction. It has been shown that these parasitic strips would not affect antennas with vertical polarization.

The effect of several parameters in the radiation pattern has also been studied, such as the angle of the strip layers, the

This article has been accepted for publication in a future issue of this journal, but has not been fully edited. Content may change prior to final publication. Citation information: DOI 10.1109/TAP.2019.2900407, IEEE Transactions on Antennas and Propagation

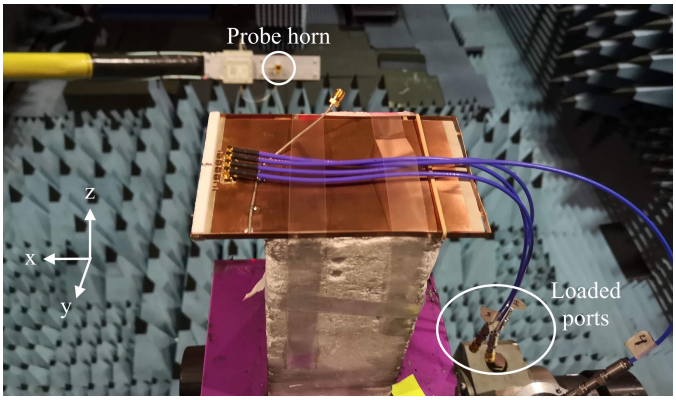

Fig. 18. Measurement set-up in the anechoic chamber.

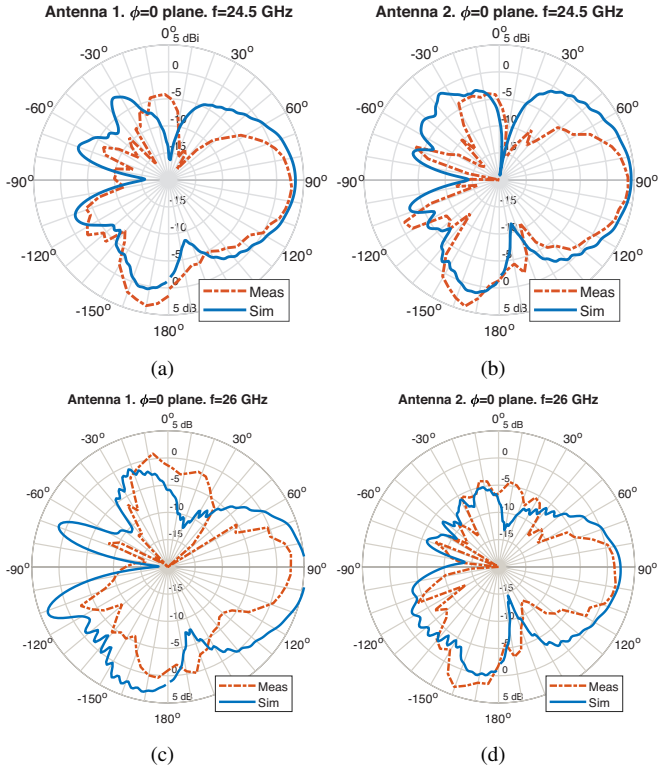

Fig. 19. Comparison of the radiation pattern of the elements in the H-plane at 24.5 GHz and 26 GHz.

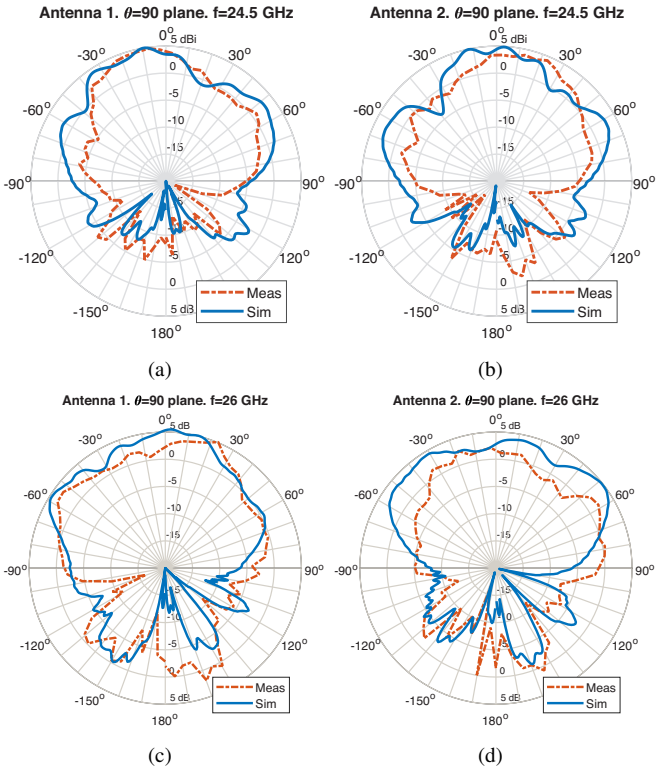

Fig. 20. Comparison of the radiation pattern of the elements in the E-plane at 24.5 GHz and 26 GHz.

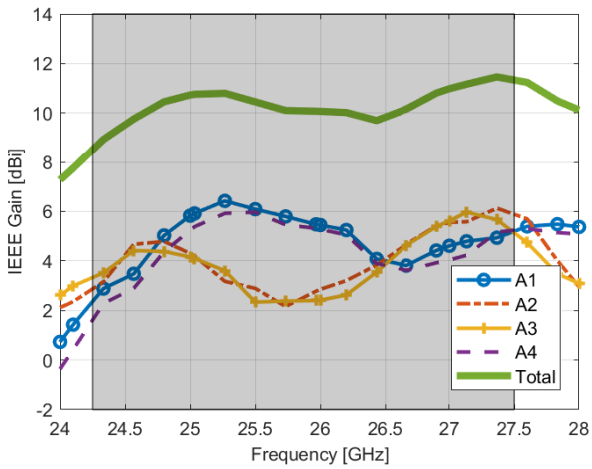

Fig. 21. Simulated realized gain in the end-fire direction ($+x$ axis), of all the antenna elements and in-phase combination of the array, in the frequency range.

gap between the strips, the strip length and the antenna-frame distance. The most critical parameters have been shown to be the gap and the strip length. The introduced metal strip layers have been shown to be able to cooperate with microstrip patches and Vivaldi antenna elements. For the final design, the mm-wave array is built of four Vivaldi elements since they provide a robust radiation pattern besides their broad bandwidth. The array is able to steer the beam from $\phi = \pm 60°$, with a realized gain higher than 7 dBi. The mm-wave array has been combined with a double-loop low-frequency antenna to present a complete prototype of a 5G-enabled handset. The low-frequency antenna serves as well as the metal frame of the terminal.

Measured results have verified the simulations. The resulting mm-wave array is matched between 24 and 27.5 GHz. The coupled metal strip layers successfully point the beam in the end-fire direction, as the radiation pattern from the antenna elements shows. Good agreement between the simulated and measured results is also found with the low-frequency antenna, that covers the frequency bands 822-995 MHz and 1338-2780 MHz.

ACKNOWLEDGMENT

The authors would like to thank the invaluable help of Ben Krøyer and Peter Jensen with the antenna manufacturing,

This article has been accepted for publication in a future issue of this journal, but has not been fully edited. Content may change prior to final publication. Citation information: DOI 10.1109/TAP.2019.2900407, IEEE Transactions on Antennas and Propagation

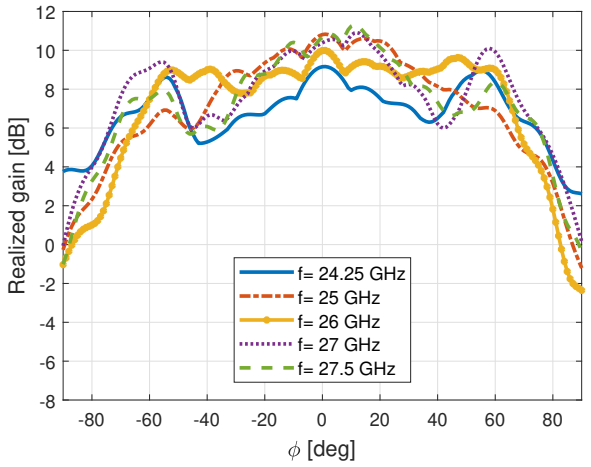

Fig. 22. Simulated realized gain beam-steering envelope.

Kristian Bank and Kim Olsen for the chamber set-up, and Igor Syrytsin and Carla Di Paola for their help with the measurements.

REFERENCES

[1] W. Hong, K.-H. Baek, Y. Lee, Y. Kim, and S.-T. Ko, "Study and prototyping of practically large-scale mmwave antenna systems for 5g cellular devices," *IEEE Communications Magazine*, vol. 52, no. 9, pp. 63–69, 2014.

[2] T. S. Rappaport, S. Sun, R. Mayzus, H. Zhao, Y. Azar, K. Wang, G. N. Wong, J. K. Schulz, M. Samimi, and F. Gutierrez, "Millimeter wave mobile communications for 5g cellular: It will work!" *IEEE Access*, vol. 1, pp. 335–349, 2013.

[3] Z. Pi and F. Khan, "An introduction to millimeter-wave mobile broadband systems," *IEEE communications magazine*, vol. 49, no. 6, 2011.

[4] J. Lee, E. Tejedor, K. Ranta-aho, H. Wang, K.-T. Lee, E. Semaan, E. Mohyeldin, J. Song, C. Bergljung, and S. Jung, "Spectrum for 5g: Global status, challenges, and enabling technologies," *IEEE Communications Magazine*, vol. 56, no. 3, pp. 12–18, 2018.

[5] S. Zhang, I. Syrytsin, and G. F. Pedersen, "Compact beam-steerable antenna array with two passive parasitic elements for 5g mobile terminals at 28 ghz," *IEEE Transactions on Antennas and Propagation*, pp. 1–1, 2018.

[6] Y. Li and Z.-C. Hao, "A wideband switched beam antenna for full 360 coverage," in *2017 Sixth Asia-Pacific Conference on Antennas and Propagation (APCAP)*. IEEE, 2017, pp. 1–3.

[7] J. Bang, Y. Hong, and J. Choi, "Mm-wave phased array antenna for whole-metal-covered 5g mobile phone applications," in *Antennas and Propagation (ISAP), 2017 International Symposium on*. IEEE, 2017, pp. 1–2.

[8] Z. Ying, K. Zhao, T. Bolin, J. Helander, D. Sjöberg, S. He, A. Scannavini, L. J. Foged, and G. Nicolas, "Study of phased array in ue for 5g mm wave communication system with consideration of user body effect," in *2016 10th European Conference on Antennas and Propagation (EuCAP)*, April 2016, pp. 1–2.

[9] H. Xia, J. Lei, L. Meng, and G. Yang, "Design and analysis of a compact reconfigurable phased antenna array with 3d coverage for 5g applications in portable devices," in *2016 Progress in Electromagnetic Research Symposium (PIERS)*, Aug 2016, pp. 2459–2463.

[10] N. Ojaroudiparchin, M. Shen, S. Zhang, and G. F. Pedersen, "A switchable 3-d-coverage-phased array antenna package for 5g mobile terminals," *IEEE Antennas and Wireless Propagation Letters*, vol. 15, pp. 1747–1750, 2016.

[11] M. Stanley, Y. Huang, H. Wang, H. Zhou, A. Alieldin, and S. Joseph, "A capacitive coupled patch antenna array with high gain and wide coverage for 5g smartphone applications," *IEEE Access*, vol. 6, pp. 41 942–41 954, 2018.

[12] S. Zhang, X. Chen, I. Syrytsin, and G. F. Pedersen, "A planar switchable 3-d-coverage phased array antenna and its user effects for 28-ghz mobile terminal applications," *IEEE Transactions on Antennas and Propagation*, vol. 65, no. 12, pp. 6413–6421, 2017.

[13] I. Syrytsin, S. Zhang, G. F. Pedersen, and A. Morris, "Compact quad-mode planar phased array with wideband for 5g mobile terminals," *IEEE Transactions on Antennas and Propagation*, 2018.

[14] J. Helander, K. Zhao, Z. Ying, and D. Sjöberg, "Performance analysis of millimeter-wave phased array antennas in cellular handsets," *IEEE Antennas and wireless propagation letters*, vol. 15, pp. 504–507, 2016.

[15] I. Syrytsin, S. Zhang, G. Pedersen, K. Zhao, T. Bolin, and Z. Ying, "Statistical investigation of the user effects on mobile terminal antennas for 5g applications," *IEEE Transactions on Antennas and Propagation*, 2017.

[16] M. M. S. Taheri, A. Abdipour, S. Zhang, and G. F. Pedersen, "Integrated millimeter-wave wideband end-fire 5g phased array and low-frequency 4g lte antenna in mobile terminals," submitted.

[17] M. Keshavarz Hedayati and M. Elbahri, "Antireflective coatings: Conventional stacking layers and ultrathin plasmonic metasurfaces, a mini-review," *Materials*, vol. 9, no. 6, p. 497, 2016.

[18] B. Yu, K. Yang, G. Yang *et al.*, "A novel 28 ghz beam steering array for 5g mobile device with metallic casing application," *IEEE Transactions on Antennas and Propagation*, vol. 66, no. 1, pp. 462–466, 2018.

[19] J. Bang and J. Choi, "A sar reduced mm-wave beam-steerable array antenna with dual-mode operation for fully metal-covered 5g cellular handsets," *IEEE Antennas and Wireless Propagation Letters*, 2018.

[20] 3GPP, "User Equipment (UE) radio transmission and reception; Part 2: Range 2 Standalone (Release 15)," 3rd Generation Partnership Project (3GPP), Technical Specification (TS) 38.101-2, 06 2018, version 15.0.0.

[21] Y.-L. Ban, Y.-F. Qiang, Z. Chen, K. Kang, and J.-H. Guo, "A dual-loop antenna design for hepta-band wwan/lte metal-rimmed smartphone applications," *IEEE Transactions on Antennas and Propagation*, vol. 63, no. 1, pp. 48–58, 2015.

[22] E. Holzman, "On the use of dummy elements to match edge elements in transmit arrays," in *Phased Array Systems & Technology, 2013 IEEE International Symposium on*. IEEE, 2013, pp. 549–552.

[23] J. H. Shafieha, J. Nourinia, and C. Ghobadi, "Probing the feed line parameters in vivaldi notch antennas," *Progress In Electromagnetics Research*, vol. 1, pp. 237–252, 2008.

[24] P. Liu, X. Zhu, X. Wang, and L. Tian, "A siw-based vivaldi array antenna for 5g wireless communication systems," in *Antennas and Propagation & USNC/URSI National Radio Science Meeting, 2017 IEEE International Symposium on*. IEEE, 2017, pp. 529–530.

Rocio Rodriguez-Cano was born in Granada (Spain) in 1993. She received the B.S. degree and MsC. in Electrical Engineering at the University of Malaga, Spain, in 2015 and 2017, respectively. She is currently pursuing a Ph.D. in antenna systems for the next generation of mobile terminals at Aalborg University, Denmark. Her current research interests include antenna design for 5G communications, integration with the former generations of mobile communications and user exposure.

Shuai Zhang (SM'18) received the B.E. degree from the University of Electronic Science and Technology of China, Chengdu, China, in 2007 and the Ph.D. degree in electromagnetic engineering from the Royal Institute of Technology (KTH), Stockholm, Sweden, in 2013. After his Ph.D. studies, he was a Research Fellow at KTH. In April 2014, he joined Aalborg University, Denmark, where he currently works as Associate Professor. In 2010 and 2011, he was a Visiting Researcher at Lund University, Sweden and at Sony Mobile Communications AB, Sweden, respectively. He was also an external antenna specialist at Bang & Olufsen, Denmark from 2016-2017. He has coauthored over 50 articles in well-reputed international journals and over 15 (US or WO) patents. His current research interests include: mobile terminal mmwave antennas, biological effects, CubeSat antennas, Massive MIMO antenna arrays, UWB wind turbine blade deflection sensing, and RFID antennas.

Kun Zhao received the B.S. degree in Communication Engineering from Beijing University of Posts and Telecommunications (BUPT), Beijing, China in 2010, M.S. in wireless systems and Ph.D. degree in electromagnetic engineering from Royal Institute of Technology (KTH), Stockholm, Sweden, in 2012 and 2017, respectively. Currently, he is a researcher of antenna technology and standardization in the Radio Access Lab, Sony Mobile Communication AB, Lund, Sweden. He also works as an industrial post-doc at Aalborg University, Denmark. He was a visiting researcher at the Department of Electrical and Information Technology, Lund University, Sweden. His current research interests include mm-wave antenna and propagation for 5G communications, MIMO antenna systems, user body interactions, and body centric wireless communications.

Gert Frølund Pedersen was born in 1965. He received the B.Sc. and E.E. (Hons.) degrees in electrical engineering from the College of Technology in Dublin, Dublin Institute of Technology, Dublin, Ireland, in 1991, and the M.Sc.E.E. and Ph.D. degrees from Aalborg University, Aalborg, Denmark, in 1993 and 2003, respectively. Since 1993, he has been with Aalborg University where he is a Full Professor heading the Antennas, Propagation and Millimeter-wave Systems LAB with 25 researchers. He is also the Head of the Doctoral School on wireless communication with some 40 Ph.D. students enrolled. His research interests include radio communication for mobile terminals especially small antennas, diversity systems, propagation, and biological effects. He has published more than 500 peer reviewed papers, 6 books, 12 book chapters and holds over 50 patents. He has also worked as a Consultant for developments of more than 100 antennas for mobile terminals including the first internal antenna for mobile phones in 1994 with lowest SAR, first internal triple-band antenna in 1998 with low SAR and high TRP and TIS, and lately various multiantenna systems rated as the most efficient on the market. He has worked most of the time with joint university and industry projects and have received more than 21 M$ in direct research funding. He is currently the Project Leader of the RANGE project with a total budget of over 8 M$ investigating high performance centimetre/millimetre-wave antennas for 5G mobile phones. He has been one of the pioneers in establishing over-the-air measurement systems. The measurement technique is now well established for mobile terminals with single antennas and he was chairing the various COST groups with liaison to 3GPP and CTIA for over-the-air test of MIMO terminals. He is currently involved in MIMO OTA measurement.